Magnetic Resonance in Medicine 43:160–162 (2000)

k-Space Partition Diagrams: A Graphical Tool for Analysis of MRI Pulse Sequences

Robert W. Cox*

A new type of graphical tool for explaining and analyzing magnetic resonance imaging pulse sequences is developed and illustrated. This tool combines the partition diagram, which shows the evolution of multiple echoes with the application of multiple RF pulses, and *k*-space graphs, which show the evolution of the transverse magnetization as gradients are applied. The strength of the new tool lies in its ability to depict clearly the progression of complex imaging pulse sequences. Several complicated excitation sequences are used to illustrate this method. Magn Reson Med 43:160–162, 2000. © **2000 Wiley-Liss, Inc.**

Key words: MRI; spin echo; *k*-space

One of the most fruitful ways to think about NMR is in terms of ''echoes'': relatively large amplitude signals produced when the phases of some portion of the transverse magnetization become approximately equal across the sample (1). Multiple RF pulses can produce multiple echoes (2). The proliferation of potential echoes in a complicated pulse sequence has previously been graphically represented by partition diagrams (3) and by an extended phase diagram (4). In these similar displays, the abscissa represents time and the ordinate is a schematic representation of the spatial coherence of components of the magnetization.

One of the most useful ways to think about MRI is in terms of ''*k*-space'': a representation of the evolution of the spatial distribution of the transverse magnetization by a trajectory scanning part of the **k** plane, during the application of field gradients (5). In this display, the abscissa and ordinate are k_x and k_y; time is represented by tracing the path followed by the transverse magnetization as gradients are applied. An echo corresponds to the time at which (k_x, k_y) passes through (or comes closest to) the origin.

These two types of diagrams illustrate different aspects of the MRI excitation and acquisition process. The principal goal of this paper is to provide a graphical combination of the partition-type diagrams, which depict multiple echo creation and evolution as multiple RF pulses are applied, and of the *k*-space diagram, which depicts the image acquisition process. The ''*k*-space partition diagram'' introduced herein is useful for explaining how different echoes (desired or unwanted) may come into focus during the image acquisition sequence.

EVOLUTION OF MAGNETIZATION

Combined Effects of RF and Gradients

The magnetization density at any given location is normally represented as a real 3-vector: $\mathbf{M} = [M_x, M_y, M_z]^T$, but for many purposes is more conveniently represented as a hybrid complex-real vector: $\mathbf{M} = [M_\perp, M_z]^T$, where $M_\perp = M_x + iM_y$. These two representations will be used interchangeably.

Consider first a spatial distribution of magnetization given by

$$\mathbf{M}(\mathbf{x}, t = 0) = \begin{bmatrix} M_\perp^{(0)} \\ M_z^{(0)} \end{bmatrix};$$

that is, uniform excitation of a slice (or volume, if **k** and **x** are 3-vectors). The application of gradient fields gives (ignoring all relaxation effects)

$$\mathbf{M}(\mathbf{x}, t) = \begin{bmatrix} M_\perp^{(0)} \\ 0 \end{bmatrix} e^{-i\mathbf{k}_0(t)\cdot\mathbf{x}} + \begin{bmatrix} 0 \\ M_z^{(0)} \end{bmatrix} e^{-i\mathbf{0}\cdot\mathbf{x}}, \qquad [1]$$

where $\mathbf{k}_0(t) = \gamma \int_0^t \mathbf{G}(\tau)\, d\tau$. In general, we could write the magnetization state at any given time as

$$\mathbf{M}(\mathbf{x}, t) = \sum_{n=1}^{N} \begin{bmatrix} M_\perp^{(n)} \\ M_z^{(n)} \end{bmatrix} e^{-i\mathbf{k}_n(t)\cdot\mathbf{x}}, \qquad [2]$$

where N is the number of components (or partitions) present. The vector magnitude of the n^{th} component is $[M_\perp^{(n)}, M_z^{(n)}]^T$, where $M_\perp^{(n)}$ is a complex constant and $M_z^{(n)}$ is a real constant. The wavenumbers $\mathbf{k}_n(t)$ of each component will differ, depending on when the components were created.

The application of an RF pulse will change the number and amplitudes of the magnetization components. For example, suppose the RF pulse rotates **M** by angle α about the x-axis. In the real notation,

$$\begin{bmatrix} M_x \\ M_y \\ M_z \end{bmatrix}_{\text{after}} = \begin{bmatrix} 1 & 0 & 0 \\ 0 & \cos\alpha & -\sin\alpha \\ 0 & \sin\alpha & \cos\alpha \end{bmatrix} \begin{bmatrix} M_x \\ M_y \\ M_z \end{bmatrix}_{\text{before}}. \qquad [3]$$

However, the evolution of **M** under gradients is most simply expressed in the complex-real notation, as in Eq. [1]. For this reason, it is very convenient to express the rotation Eq. [3] in the complex-real notation. This can be done by including the complex conjugate of **M** in the

Biophysics Research Institute, Medical College of Wisconsin, Milwaukee, Wisconsin.

Grant sponsor: National Institutes of Health; Grant numbers: MH51358; NS34798.

*Correspondence to: Robert W. Cox, Biophysics Research Institute, Medical College of Wisconsin, 8701 Watertown Plank Road, Milwaukee, WI 53226. E-mail: rwcox@mcw.edu

Received 22 January 1999; revised 12 July 1999; accepted 15 September 1999.

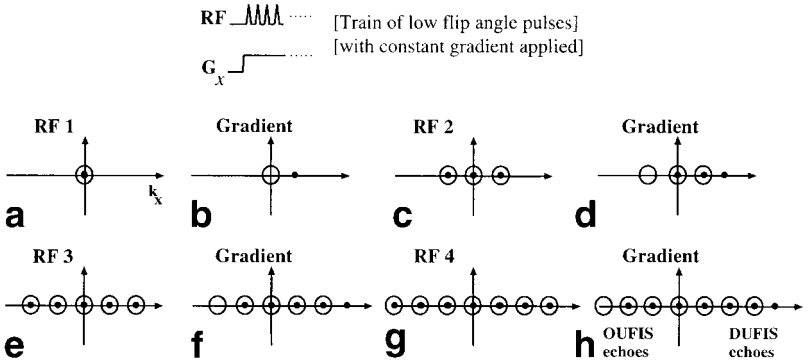

FIG. 1. DUFIS/OUFIS excitation: a train of low flip angle RF pulses is applied while a constant G_x gradient field is applied. Subfigures **a–h** show the evolution of the magnetization in *k*-space as the RF pulses and gradient field affect **M**. Solid dots represent transverse magnetization; hollow circles represent longitudinal magnetization. In DUFIS, the $k_x > 0$ echoes at **h** are subsequently used to form an image; in OUFIS, the $k_x < 0$ echoes are optimized, by selection of appropriate RF, for the image formation process.

expression, since $M_x = \frac{1}{2}(M_\perp + M_\perp^*)$ and $M_y = 1/2i\,(M_\perp - M_\perp^*)$:

$$\begin{bmatrix} M_\perp \\ M_z \end{bmatrix}_{\text{after}} = \begin{bmatrix} \cos^2(\frac{1}{2}\alpha) & \sin^2(\frac{1}{2}\alpha) & -i\sin\alpha \\ -\frac{1}{2}i\sin\alpha & \frac{1}{2}i\sin\alpha & \cos\alpha \end{bmatrix} \begin{bmatrix} M_\perp \\ M_\perp^* \\ M_z \end{bmatrix}_{\text{before}} . \quad [4]$$

Allowing for the spatially dependent phase factor $\exp[-i\mathbf{k}_n(t)\cdot\mathbf{x}]$ in each term, the magnetization of Eq. [2] becomes, after the RF pulse,

$$M_{\perp,\text{after}}(\mathbf{x}) = \sum_n \left([\cos^2(\tfrac{1}{2}\alpha)M^{(n)}_{\perp,\text{before}} - i\sin\alpha M^{(n)}_{z,\text{before}}]\, e^{-i\mathbf{k}_n\cdot\mathbf{x}} + \sin^2(\tfrac{1}{2}\alpha)M^{(n)*}_{\perp,\text{before}} e^{+i\mathbf{k}_n\cdot\mathbf{x}}\right) \quad [5a]$$

$$M_{z,\text{after}}(\mathbf{x}) = \sum_n \left([-\tfrac{1}{2}i\sin\alpha M^{(n)}_{\perp,\text{before}} + \cos\alpha M^{(n)}_{z,\text{before}}]e^{-i\mathbf{k}_n\cdot\mathbf{x}} + \tfrac{1}{2}i\sin\alpha M^{(n)*}_{\perp,\text{before}} e^{+i\mathbf{k}_n\cdot\mathbf{x}}\right) . \quad [5b]$$

The $\exp[+i\mathbf{k}_n\cdot\mathbf{x}]$ terms in [5] arise from the $M_\perp^*$ component in [4]. Equations [1] and [5] together describe the evolution of a magnetization field (Eq. [2]) that comprises a finite number of components. Note that the number of components N will in general change after the application of the RF pulse (unless $\alpha = 180°$).

Graphical Representation

In the pictorial representation adopted here, solid dots are used to represent transverse magnetization components ($M_\perp \exp[-i\mathbf{k}\cdot\mathbf{x}]$). Larger hollow circles are used to represent longitudinal magnetization components ($M_z \exp[-i\mathbf{k}\cdot\mathbf{x}]$; these will occur in $\pm\mathbf{k}$ pairs, so that the net M_z is real). The solid dots and hollow circles are overlaid when the components occur at the same value of **k**.

Under the application of gradients and RF pulses, the solid dots and hollow circles will change. The rules for evolution of these markers are:

Gradients:

All solid dots move, with the same velocity $d\mathbf{k}/dt = \gamma\mathbf{G}(t)$.

The hollow circles do not move.

RF(α) about *x*:

A solid dot at wavenumber **k** breaks into four components:

(a) solid at **k** with amplitude $\cos^2(\frac{1}{2}\alpha)\,M_\perp$
(b) solid at $-\mathbf{k}$ with amplitude $\sin^2(\frac{1}{2}\alpha)\,M_\perp^*$
(c) hollow at **k** with amplitude $-\frac{1}{2}i\sin\alpha M_\perp$
(d) hollow at $-\mathbf{k}$ with amplitude $\frac{1}{2}i\sin\alpha M_\perp^*$

A hollow circle at wavenumber **k** breaks into two components:

(e) solid at **k** with amplitude $-i\sin\alpha M_z$
(f) hollow at **k** with amplitude $\cos\alpha M_z$

(For RF about a general axis, the split-up rules are similar, but with more complicated formulas for the resulting amplitudes.) Note that with a slice-selective RF pulse, the flip angle α will be a function of the through-slice coordinate *z*. As is well known, this effect can produce unwanted echoes from the fringes of the slice.

Figure 1 shows an example of this representation applied to the DANTE Ultrafast Imaging Sequence (DUFIS) (6) and Optimized Ultrafast Imaging Sequence (OUFIS) (7) excitation sequences. Figure 2 shows the representation of the Spatial Modulation of Magnetization (SPAMM) (8) excitation of a sinusoidal grating in $M_\perp$. Both of these pulse sequences involve a mixture of multiple RF pulses with gradients.

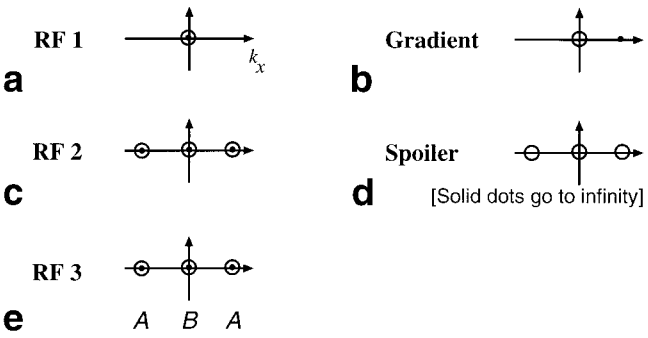

FIG. 2. SPAMM excitation: RF is applied, then a gradient G_x, then RF, then a spoiler gradient, then RF again. At subfigure **e**, $M_\perp(x, y) = A(e^{-ikx} + e^{+ikx}) + B = B + 2A\cos kx$, giving a sinusoidal grating. Subsequent gradients (not shown) move the solid dots around *k*-space together, producing an image with dark bands overlaid.

The principal drawback of this new type of diagram is that it is time-dependent. Too much information is presented on each graph to easily show all points in time in one display. The more qualitative extended phase diagram (4) can be used when a single graph is needed.

REFERENCES

1. Hahn EL. Spin Echoes. Phys Rev 1950;80:580–594.
2. Woessner DE. Effects of diffusion in nuclear magnetic resonance spin-echo experiments. J Chem Phys 1961;34:2057–2061.
3. Kaiser R, Bartholdi E, Ernst RR. Diffusion and field-gradient effects in NMR Fourier spectroscopy. J Chem Phys 1974;60:2966–2979.
4. Hennig J. Multiecho imaging sequences with low refocusing flip angles. J Magn Reson 1988;78:397–407.
5. Ljunggren S. A simple graphical representation of Fourier-based imaging methods. J Magn Reson 1983;54:338–343.
6. Lowe IJ, Wysong RE. DANTE Ultrafast Imaging Sequence (DUFIS). J Magn Reson 1993;101:106–109.
7. Zha L, Lowe IJ. Optimized ultra-fast imaging sequence (OUFIS). Magn Reson Med 1995;33:377–395.
8. Axel L, Dougherty L. MR imaging of motion with spatial modulation of magnetization. Radiology 1989;171:841–845.